Spatially selective 2D RF inner field of view (iFOV) diffusion kurtosis imaging (DKI) of the pediatric spinal cord

Chris J. Conklin[a,h,*], Devon M. Middleton[b,c], Mahdi Alizadeh[b,c], Jürgen Finsterbusch[d], David L. Raunig[e], Scott H. Faro[b,c], Pallav Shah[b], Laura Krisa[f,g], Rebecca Sinko[g], Joan Z. Delalic[a], M.J. Mulcahey[g], Feroze B. Mohamed[c,h]

[a]Electrical Engineering, Temple University, Philadelphia, PA, United States
[b]Radiology, Temple University, Philadelphia, PA, United States
[c]Bioengineering, Temple University, Philadelphia, PA, United States
[d]Systems Neuroscience, University Medical Center Hamburg-Eppendorf, Hamburg, Germany
[e]ICON Medical Imaging, Warrington, PA, United States
[f]Physical Therapy, Thomas Jefferson University, Philadelphia, PA, United States
[g]Occupational Therapy, Thomas Jefferson University, Philadelphia, PA, United States
[h]Radiology, Thomas Jefferson University, Philadelphia, PA, United States

ARTICLE INFO

ABSTRACT

Magnetic resonance based diffusion imaging has been gaining more utility and clinical relevance over the past decade. Using conventional echo planar techniques, it is possible to acquire and characterize water diffusion within the central nervous system (CNS); namely in the form of Diffusion Weighted Imaging (DWI) and Diffusion Tensor Imaging (DTI). While each modality provides valuable clinical information in terms of the presence of diffusion and its directionality, both techniques are limited to assuming an ideal Gaussian distribution for water displacement with no intermolecular interactions. This assumption neglects pathological processes that are not Gaussian therefore reducing the amount of potentially clinically relevant information. Additions to the Gaussian distribution measured by the excess kurtosis, or peakedness, of the probabilistic model provide a better understanding of the underlying cellular structure. The objective of this work is to provide mathematical and experimental evidence that Diffusion Kurtosis Imaging (DKI) can offer additional information about the micromolecular environment of the pediatric spinal cord. This is accomplished by a more thorough characterization of the nature of random water displacement within the cord. A novel DKI imaging sequence based on a tilted 2D spatially selective radio frequency pulse providing reduced field of view (FOV) imaging was developed, implemented, and optimized on a 3 Tesla MRI scanner, and tested on pediatric subjects (healthy subjects: 15; patients with spinal cord injury (SCI):5). Software was developed and validated for post processing of the DKI images and estimation of the tensor parameters. The results show statistically significant differences in mean kurtosis ($p < 0.01$) and radial kurtosis ($p < 0.01$) between healthy subjects and subjects with SCI. DKI provides incremental and novel information over conventional diffusion acquisitions when coupled with higher order estimation algorithms.

1. Introduction

The process of diffusion is a random walk phenomenon and as such can be governed by a probabilistic distribution. Traditional diffusion and diffusion tensor imaging (DTI) assumes an ideal Gaussian form of water displacement regardless of the surrounding microenvironment. This is a limiting assumption as tissue geometry and cellular barriers will necessarily alter the path of diffusion. In contradistinction, Diffusion Kurtosis Imaging (DKI) attempts to quantify the divergence of water diffusion from the ideal Gaussian probabilistic model. By measuring excess kurtosis a more thorough characterization of tissue complexity can be obtained as the underlying diffusion distribution can more accurately reflect the presence of diffusion barriers local to the imaging volume (Jensen et al., 2005; Jensen and Helpern, 2003; Lu et al., 2006). Kurtosis is defined as the shift of probability mass from the shoulders of a distribution to its center and tails, which is mathematically depicted below:

$$K = \beta_2 - 3 \frac{\mu_4}{\mu_2^2} - 3 \frac{\langle x^4 \rangle}{\langle x^2 \rangle^2} - 3.$$

Because it does not consider kurtosis in the water diffusion distribution, DTI offers information related to the magnitude and direction of

* Corresponding author at: Thomas Jefferson University, 909 Walnut Street, Philadelphia, PA 19107, United States.
E-mail address: Christopher.conklin@jefferson.edu (C.J. Conklin).

diffusion but lacks the ability to detect microenvironment viscosity and/or diffusional barriers (Jensen et al., 2005; Lu et al., 2006; Jensen and Helpern, 2010; Bester et al., 2010). In addition, the conventional diffusion tensor cannot accurately resolve fiber crossings due to its lack of ability to completely characterize the diffusion process (Lazar et al., 2008). The concept of quantifying and characterizing the diffusion profile of different structures has been around for some time in the form of q-space imaging (QSI) (Cohen and Assaf, 2002; Latt et al., 2008). While QSI can completely detail the diffusion displacement of water, it lacks clinical significance at this time due to the need for high gradient strength systems and longer imaging sessions, which makes it not suitable for clinical imaging (Lu et al., 2006; Jensen and Helpern, 2010; Hori et al., 2012). However, Jensen and Helpern (Jensen et al., 2005; Jensen and Helpern, 2010) noticed that the application of large gradient fields introduced signal nonlinearity in the brain subsequently hinting at the presence of kurtosis (Jensen and Helpern, 2003). By incorporating the quadratic term of the diffusion signal polynomial expansion, it was possible to get a more complete characterization of the diffusion process, namely the kurtosis, while still remaining clinically feasible in terms of scan duration and hardware requirements (Jensen et al., 2005).

The introduction of the kurtosis tensor in the model requires the addition of at minimum one extra b-value, which should not exceed 3000 mm/s^2 (Lu et al., 2006), and at least 30 gradient directions (15 directions per b-value). This high angular resolution is needed to characterize the kurtosis tensor. As was previously stated, QSI can provide this information but the need for high b-values, which in turn results in a lower signal to noise ratio (SNR) due to the more rapid signal dephasing process make it infeasible. In contradistinction, DKI can be used to calculate kurtosis metrics as well as the orientation distribution function of the diffusion distribution regardless of the model used (Lazar et al., 2008). Simply stated, DKI is a refinement of DTI with DTI being a first order approximation and DKI being second order. Non-zero kurtosis may indicate single compartment voxels with barriers or multi-compartment voxels with normal Gaussian displacements within the compartment having different diffusion coefficients (Lu et al., 2006). In essence, no assumptions are made about the compartmental nature within voxels. This allows for a relatively unrestricted investigation as to the nature of diffusion through the presence of barriers.

Recent work has investigated DKI in the adult brain and the spinal cord and it is gaining momentum in the study of pediatrics populations. Multiple sclerosis (MS) patients have been studied in an adult population within these regions (Bester et al., 2010; Raz et al., 2013; Yoshida et al., 2013). Given that kurtosis is sensitive to structural changes in isotropic tissues it served as an ideal technique for looking at normal appearing tissue within this patient population. Significant work is also being performed to investigate the pediatric brain, particularly age related developmental microstructural gray and white matter changes as well as epilepsy (Paydar et al., 2014; Li et al., 2012; Zhang et al., 2013). Interestingly, kurtosis metrics all continued to increase with age even as fractional anisotropy (FA) values plateau. This result is profound in that isotropic microenvironments continued to evolve and develop even after white matter pathways were established suggesting a higher degree of structure in gray matter than offered by DTI (Paydar et al., 2014).

Recently, spinal cord DKI was performed on adult patients with cervical spondylosis, a degenerative process which can lead to motor and sensory dysfunction (Hori et al., 2014). Thirteen patients with cervical myelopathy were recruited to investigate microstructural changes in gray and white matter. Tract specific analysis was performed but only gray matter mean kurtosis (MK) demonstrated statistically significant differences between affected versus unaffected cords. Affected cords had an MK of 0.6 ± 0.18 while unaffected cord had a MK of 0.73 ± 0.13 with a p-value of 0.0005. This study used an outer volume suppression (OVS) inner field of view technique for data collection (Wilm et al., 2007; Wilm et al., 2009). This appears to be the only published study that has incorporated this imaging strategy into a DKI protocol. In contrast, the current work incorporated a novel tilted 2D RF spatially selective reduced field of view method to reduce in plane distortions and obtain reliable DKI data. To our knowledge this is the first study to use such a pulse sequence to extract kurtosis information from the pediatric spinal cord.

Previous discussions have focused on DKI in the central nervous system (CNS), however, it is important to note that DKI has also been applied to prostate cancer for predicting adverse outcomes (Rosenkrantz et al., 2013), and to head and neck squamous cell carcinomas (Jansen et al., 2010), and kidneys (Pentang et al., 2014) to improve DWI modeling fit. It can be seen that diffusion kurtosis imaging has the potential to be versatile in terms of clinical applicability since it can yield information about the underlying micromolecular environment of any anatomical region influenced or governed by diffusional processes.

The aim of this work was to implement a novel reduced field FOV DKI sequence and to optimize the acquisition sequence in terms of scanning time and distortion minimization to investigate clinical applicability to pediatric spinal cord injury (SCI). This additional information could serve as a potential biomarker for further characterization and quantification of functional changes in the spinal cord as a result of injury. It is hypothesized that the DKI values obtained from injured cords will show statistically significant differences when compared with values obtained from uninjured, healthy cords.

2. Methods

2.1. Subject recruitment

For this study a total of 20 subjects (15 healthy subjects and 5 pediatric patients with cervical SCI) having a mean age of 10 years and 4 months (age range: 6–16) were recruited. All subjects and parents were provided informed assent and consent of the IRB-approved imaging protocol. Healthy subjects recruited for this study were typically developing children/adolescents with no evidence of spinal cord pathology or traumatic injury with a mean age of 10 years and 5 months. 10 females and 5 males made up this population. SCI patients were recruited if they had chronic cervical injury and were free of spinal instrumentation. The mean age for SCI patients was 10 years and 1 month old (4 males and 1 female). SCI subjects were excluded if their injuries were not chronic (<1 year post injury), had pace makers or other implantable electrical stimulation devices, were unable to lay supine for 45 min, required sedation to undergo an MRI, required mechanical ventilation, contained metallic fragments (such as bullets), or had suicidal ideations. Table 1 describes the MRI findings on T2 weighted images for each of the five SCI patients.

2.2. Image acquisition

Given the inherent limitations with acquiring functional data on the spinal cord, a specialized acquisition sequence was optimized. Echo-planar imaging (EPI) suffers from geometric distortions due to magnetic

Table 1
MRI findings for the five SCI subjects based on T2-weighted images.

Subject	MRI findings (T2)
SCI 1	Mild to moderate focal atrophy (C5–C6 to C7–T1); Subtle increase in intramedullary signal (mid C3 to mid C5); No hemorrhage
SCI 2	Marked focal atrophy w/large focal syringomyelia (mid C7 to mid T1); Increased intramedullary signal w/mild atrophy (mid C6 to mid C7); No hemorrhage
SCI 3	Subtle increase in intramedullary signal (C1); Increased signal of left cord (C7–T1); No atrophy; No hemorrhage
SCI 4	Mild atrophy (C6–C7 to C7–T1); No abnormal intramedullary signal; No hemorrhage
SCI 5	Tiny focus of increased intramedullary signal (C6–C7); Focal atrophy (mid C6 to C7–T1) marked at C6–C7 level; No hemorrhage

field inhomogeneities as well as susceptibility differences between adjacent anatomical structures. These distortions manifest due to accumulated phase differences along the echo train and are indistinguishable from the modulation needed for spatial encoding. Increasing the gradient blips along the phase encode direction mitigate these distortions (Finsterbusch, 2009; Rieseberg et al., 2002) and reduce the need for reduction in the field of view in the phase direction which can be achieved through the use of a 2DRF excitation profile.

This inner field of view sequence was implemented on a 3.0 T Siemens Verio MR scanner and optimized for both signal and scan duration when imaging the pediatric spinal cord. High in-plane resolution axial diffusion weighted images were acquired to cover the entire cervical spinal cord (C1–C7) using an 8 channel spine array in conjunction with a 4 channel neck coil. Imaging parameters optimized for kurtosis imaging were: 30 diffusion directions, b-values = [0 1000 2000] s/mm^2, voxel size = $0.8 \times 0.8 \times 6$ mm^3, field of view = 164×47 mm^2, axial slices = 25, TR = 5200 ms, TE = 123 ms, number of averages = 1 (with 6 B_0 images), and acquisition time = 5:48 min:sec. Conventional T1 and T2 scans were also obtained for clinical review. Anesthesia was not administered to the subjects in this study and cardiac/respiratory gating was not used to keep scan times as short as possible.

2.3. Image processing

As diffusion weighted data is analyzed at a voxel level, intrascan and/or interslice motion can be detrimental to the accuracy of the modeled results. Motion correction was performed first on the six B0 images to create a mean image and diffusion weighted images were subsequently coregistered to the mean B0 (Middleton et al., 2014). This averaging and coregistration process maximizes the signal to noise ratio (SNR) while also smoothing out spurious signal spikes.

With the data properly preprocessed, kurtosis tensor estimation was performed through the following relation:

$$\ln[S(b)] = \ln[S(0)] - bD_{app} + \frac{1}{6}b^2 D_{app}^2 K_{app} + O\left(b^3\right).$$

The above expression can be discretized and reduced to a linear least squares problem as outlined in Tabesh et al. (2011)). As the output of the linear least squares fit gives a simultaneous estimate of both the diffusion and kurtosis tensors it is required to incorporate all b-values used during acquisition ([0 1000 2000] s/mm^2) to solve this minimization problem. However, inherent signal variability can adversely affect the accuracy of the calculated results. Signal variability in diffusion imaging is introduced not only through thermal noise and system instability, but also spatial and temporal artifacts commonly referred to as physiologic noise. Physiologic phenomenon such as CSF flow, cardiac pulsation, and subject motion will precipitate signal perturbations that manifest as data outliers. These outliers can and will alter the modeled results with the potential to give an unrealistic characterization of the diffusion profile for a given imaging region. Physiologic noise has no known parametric distribution, unlike Gaussian modeled thermal noise, and as such is handled through robust estimators. Robust estimation of tensors by outlier rejection (RESTORE) is an iteratively reweighted least squares formulation that attempts to eliminate outliers through weighting out data points with large residuals (Chang et al., 2005). The RESTORE process was implemented prior to the final kurtosis and diffusion tensor estimation to ensure removal of outlier data. This is of particular importance for spinal cord imaging due to the close proximity to the heart and lungs.

2.4. ROI definition

After estimation of the diffusion and kurtosis tensors and the generation of the appropriate diffusion metric maps, regions of interest (RoI) were drawn to extract information from the whole cord (both gray and white matter). RoIs were manually drawn on FA maps at every axial level after being anatomically localized by a board certified neuroradiologist. Given the qualitative nature of the RoI definition process, every attempt was made to ensure that there was consistent sparing of the outer margin of the cord of approximately one voxel to avoid partial volume effects due to CSF contamination. This procedure was followed throughout all slices for all subjects, both healthy subjects and patients with SCI. DKI and DTI metrics were calculated at each disk level as well as the middle of each cervical vertebral body.

2.5. Statistics

Upon definition of whole cord RoIs for each calculated kurtosis and diffusion metric map, statistical analysis was performed between patient and healthy groups. A comprehensive data table was created containing slice specific RoI information for FA, MK, mean diffusivity (MD), radial kurtosis (Krad), radial diffusivity (Drad), axial kurtosis (Kax), and axial diffusivity (Dax) for each subject. A repeated measure mixture model was constructed looking at group differences by assigning RoI level and group composition as the fixed effects. The covariance matrix was modeled as unstructured and repeated based on level. This type of repeated measures analysis is advantageous as few inherent assumptions are made in regards to the data. One assumption is that the data is normally distributed at each level for each subject. It also assumes the level is a fixed effect, indicating that any differences seen between levels are the same regardless of which subgroup is being investigated (healthy/patient). A test of this assumption showed no evidence of a significant level-by-subgroup interactions. All inferences are a direct result of the model definition and data structure. This technique clusters level information by subject, using the subject as their own control and so considers only the measurement variance as the correct error and not the variance between subjects. The result is essentially a test of the signal to noise ratio as a measure of method sensitivity. The repeated measurement model tests whether there is sufficient evidence to reject that the two methods are the same and so are able to conclude that they are different beyond what may be observed by random chance due to measurement variability and not subject selection, expanding the inference beyond the selected patients to the prescribed patient population.

The model for repeatability was fit by level for each metric considering the subject as the random effect. This provides a maximum likelihood variance estimate of the residual (difference between scans 1 and 2) for the coffee break design. Using the residual variance as the measurement error enables the calculation of the minimum detectable difference (MDD), defined as the minimum difference that may be confidently detected in a single patient at a given level. An alpha of 0.05 was selected thereby suggesting that any difference greater than the MDD has a 95% chance that it was due to a real biological change in the cord. Since the MDD is defined by the residual (or pooled) measurement error, the detection applies to all patients that meet the same inclusion criteria as the patients analyzed. This is a much more informative statistic than ICC as the ICC is an aggregated statistic and, as primarily a function of sample heterogeneity, can be unusually high for highly variable subjects ($\frac{\sigma_{between}}{\sigma_{between} + \sigma_{within}}$). In essence, high values can be meaningless in practice and very high values may be solely due to sample heterogeneity. Additionally, in the absence of residual dependence on the mean, the resulting error is orthogonal, an ideal outcome.

3. Results

Visually, the generated maps of the kurtosis analysis support the notion that measuring the kurtotic distribution of the water displacement yields a more pronounced definition of different tissue types as illustrated in Fig. 1. The figure shows the diffusion and kurtosis maps of a mid-cervical slice of a healthy, typically developing
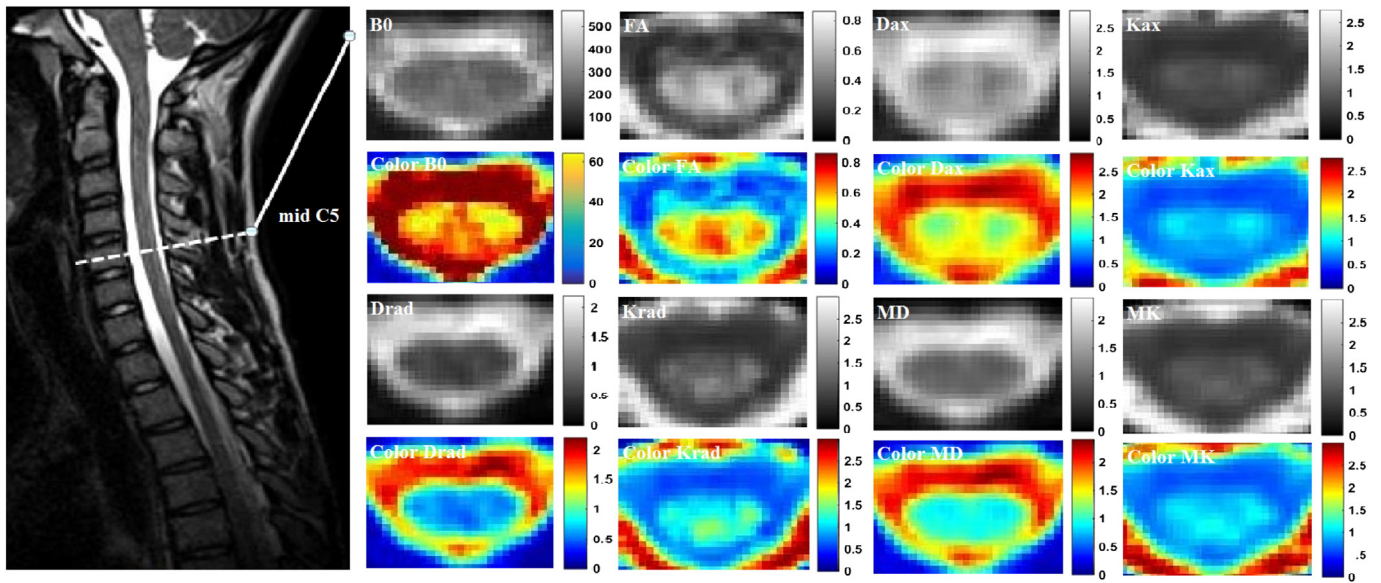
Fig. 1. Diffusion and kurtosis maps at the mid-C5 level for a healthy adolescent. Color maps are provided for visualization and help enunciate different contrast mechanisms. (For interpretation of the references to color in this figure legend, the reader is referred to the web version of this article.)

adolescent. Of particular interest is that inspection of the MK color map shows better visualization of the gray matter within the cord which is not seen in the conventional MD image for the same slice location. This ability to better define the gray and white matter may allow more accurate interrogation of various pathologies that affect the spinal cord. Fig. 2 shows the various DTI and DKI maps of an injured subject. Visually, the results at the C7–T1 level suggest the presence of a severe trauma to the spinal cord as is evident from the Bo, DKI and DTI parametric images. The three different slice locations are shown to highlight the extent of the injury.

The above methodology (Section 2) generated a series of results that help to characterize both the kurtosis and diffusion characteristics of the normal and injured pediatric spinal cords. To highlight graphical differences between the two groups, box and whisker plots were created for each estimated parameter. The first metric to be described is FA, which was included to ensure that the already established diffusion parameters generated by this algorithm are congruent with previous pediatric spinal cord work. The first data cluster in Fig. 3 depicts the group differences between healthy subjects and patients for FA.

It can be seen that typically developing pediatric cords have a FA value of roughly 0.46 with injured pediatric cords around 0.4. These value differences are statistically significant with a p-value less than 0.0001. It is important to note that there is a large variance associated with the patient group which is probably a function of the relatively low sample size (n = 5), differences between the type of injury (traumatic/nontraumatic), and severity of injury.

MK differences are shown in the second data cluster contained within Fig. 3. Again, similar to FA, patients demonstrate a lower mean kurtosis in comparison to typically developing children. Healthy subjects had a mean value of 0.9 with patients at around 0.8. These results were significantly different with a p-value of 0.0113.

Healthy subjects showed Krad values of 0.82 with patients at 0.77 with a significance level of 0.0087. Interestingly, the radial diffusivity increases in patients as shown in Fig. 3. Differences of roughly 0.2 exist between the groups with a p-value of 0.0383.

The final parameter that was investigated is the mean diffusivity, differences in which were not found to be significant. Given the lack of statistical significance that exists for the axial component, it is intuitive that
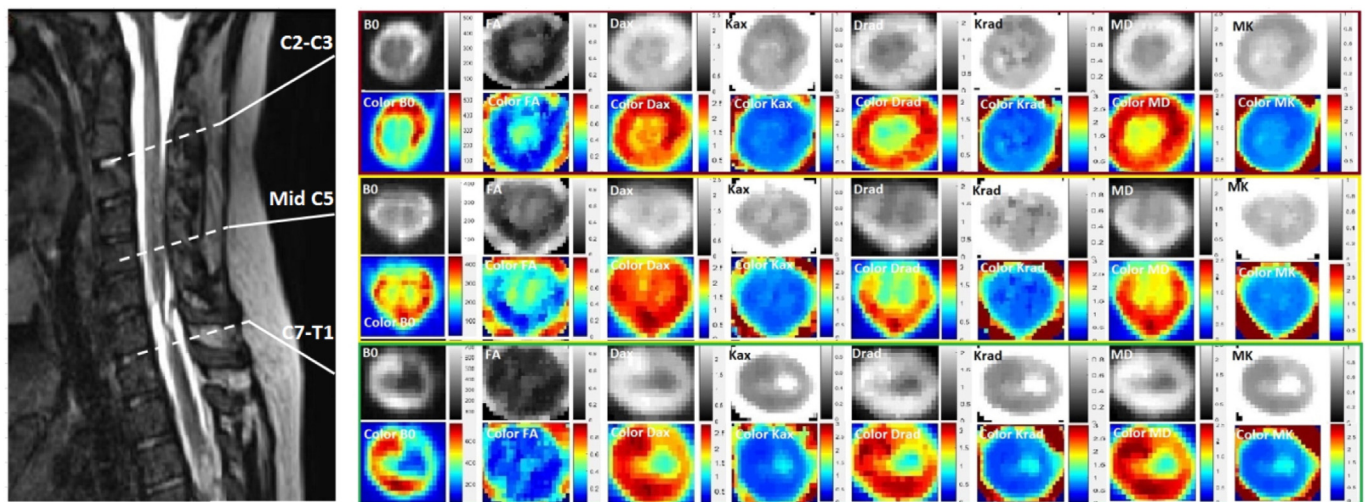

Fig. 2. Diffusion and kurtosis maps of a SCI patient showing the various maps at three different locations in the cervical cord. The functional maps at the C7–T1 level show abnormalities consistent with spinal cord trauma.
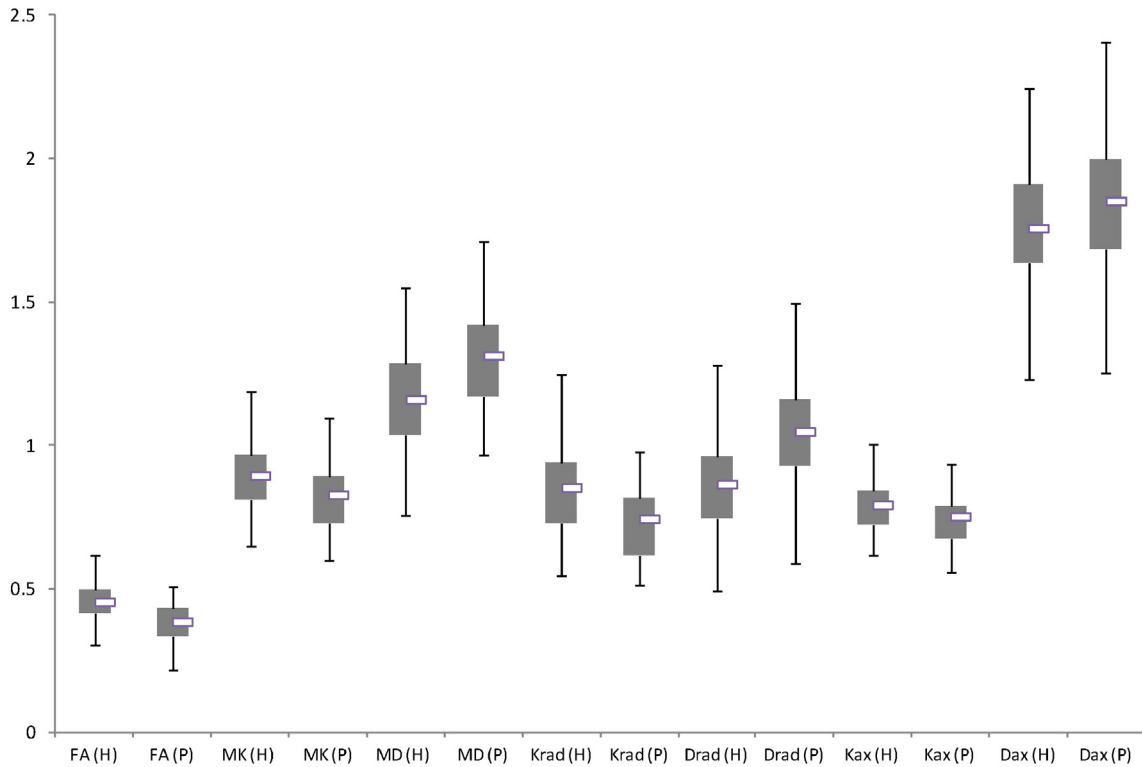
Fig. 3. Box plots for each of the seven measured diffusion parameters. Each parameter has a box plot for both healthy (H) participants and patients (P).

the mean diffusion, which is a function of both the radial and axial constituents, is not significant either.

The results from the repeated measures mixed model are summarized in Table 2.

The final results that need to be mentioned are those pertaining to the repeatability analysis. As mentioned during the statistical methodology section the following plot (Fig. 4) shows an anatomical level breakdown describing the MDD for each of the seven calculated diffusion metrics.

The repeatability results are convincing, with the FA MDD being the most sensitive at detection of an abnormal biological process as this potential biomarker requires the smallest change, while maintaining statistical significance, to differentiate healthy from pathologic tissue. Wald confidence intervals are also provided as the model definition included unbounded variance components. The asymmetry of these bounds is due to the fact that this process follows a chi-squared distribution.

4. Discussion

The results detailed in Section 3 show statistically significant differences between healthy subjects and SCI patients for FA, MK, Krad, and Drad. The FA differences follow the trend shown in previous work (Barakat et al., 2011) with patients having a lower FA relative to healthy

Table 2
Tabulation of statistical results depicted in Fig. 2. Statistically significant results are denoted with an asterisk. Units for MD and the axial/radial diffusivity are given in 10^{-3} mm^2/s.

	Healthy (n = 15)		Patients (n = 5)		Prob > |t|
	Mean	Std. Err.	Mean	Std. Err.	
MK	0.8955143	0.1268631	0.8284419	0.1537234	0.0113*
MD	1.1605821	0.1685569	1.3132117	0.2314225	0.1486
Krad	0.8529494	0.1823005	0.7436254	0.1669128	0.0087*
Drad	0.8644362	0.1688524	1.0486421	0.2287584	0.0383*
Kax	0.7929434	0.094897	0.7520648	0.1274471	0.0718
Dax	1.7575139	0.205746	1.8520006	0.2603917	0.9037
FA	0.4550699	0.0673923	0.3851518	0.0666581	0.0001*

subjects which is indicative of a more isotropic diffusion pattern due to disruption of white matter tracts. This result gives additional confidence that the in-house kurtosis software is robust enough to provide comparable results in terms of parameters calculated from conventional DTI data sets.

The decrease of MK in patients with SCI suggests the presence of structural abnormalities since kurtosis is representative of the degree of structure in an imaging volume. The closer the mean kurtosis gets to zero, the more perfectly Gaussian the diffusion profile becomes, which in the spinal cord could be indicative of disruption of the motor and sensory spinal tracts. Of particular interest and increasing importance are the investigations of the radial and axial components of kurtosis and diffusion datasets. These components may aid in determining the nature and extent of injury. The radial kurtosis, as previously stated is the in-plane kurtosis component and could be representative of the degree of axonal and myelin integrity.

These results show a similar trend consistent with the MS work previously discussed. It was shown that both the FA and MK significantly decreased with an increase in MD when comparing MS patients to healthy subjects. Also, and more interestingly, both normal appearing gray matter and white matter demonstrated a decrease in MK in patients relative to healthy subjects (Bester et al., 2010). Another more recent and larger study of MS (19 MS patients and 16 healthy subjects) in the spinal cord showed similar results (Raz et al., 2013). Results of the whole cord FA and MK as well as white matter FA and the gray matter MK were significantly decreased in patients while showing an increase in whole cord MD. This study is another example of how DTI and DKI metrics can be complimentary and jointly used for a more thorough characterization of both normal appearing and pathologic tissue in MS. While the whole cord MD did increase for this work, it was not statistically significant. However, the consistency in the trend is encouraging.

Noticing that radial kurtosis decreases while radial diffusivity increases for patients relative to healthy subjects could serve as a potential biomarker for determination of pathology and/or injury. Each biomarker, individually, provides partial information to completely quantify
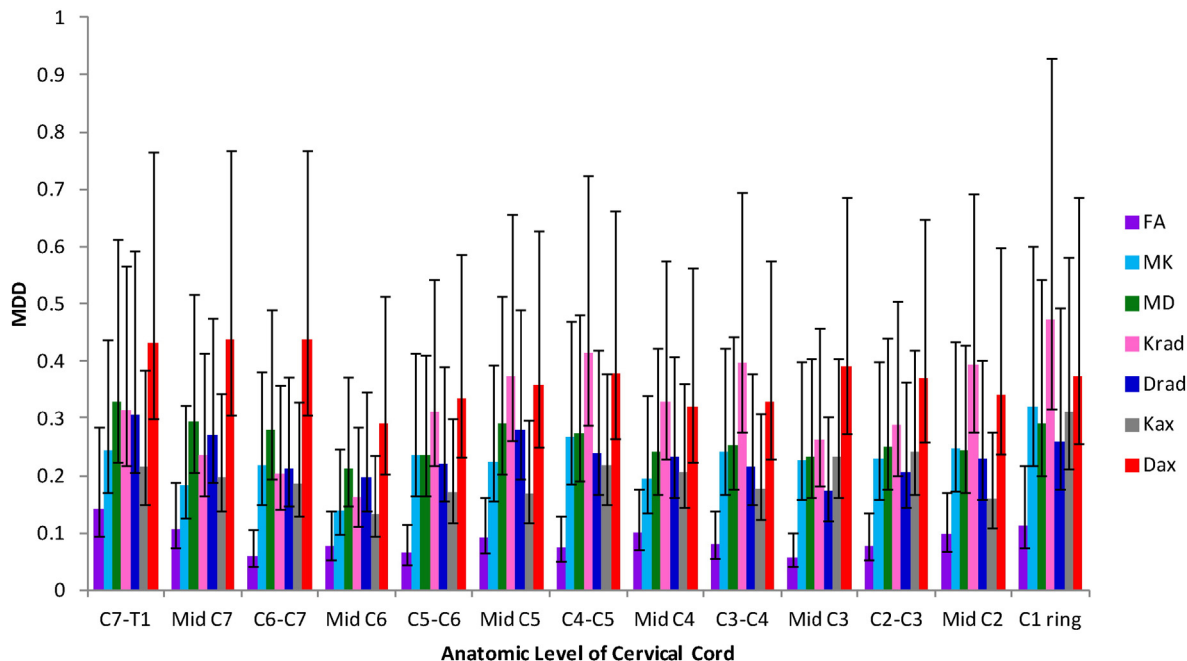
Fig. 4. Repeatability results showing the minimum detectable difference for each of the seven diffusion parameters at discrete locations along the cervical spinal cord. MDD results were calculated using $\alpha = 0.05$. Wald confidence intervals are displayed.

spinal cord pathology but are complements and add to the total information. The additional information from the multiple biomarker characterization of the pathology reduces the overall variability of the determination of positive or negative pathology and so reduces the multivariate variance when both biomarkers are used.

The lack of statistically significant differences seen for axial components of diffusion and diffusional kurtosis may suggest that the through-plane diffusion has not been altered as a result of injury. Superior to inferior and inferior to superior communication along the axons may not be substantially altered, but rather given the radial differences could be representative of a transection or shearing of the tracts at a given level due to trauma. It may be as likely that it is more difficult to detect changes in the inferior to superior direction because the axonal orientation does little to restrict diffusion in this direction in a healthy cord.

Several limitations exist for this study, primarily the relatively small sample size of the patient population ($n = 5$) as well as the type and location of the cervical injury. This was also not an age/gender matched study. The small sample size limits the ability of the results to be adequately generalized over the entire pediatric SCI population. However, the significant p-values shown in the comparison of healthy to patients was significant indicating that there is reasonably good evidence that there is a real difference and it is not likely due to chance. Additionally, the standard deviations for both healthy and patients are consistent between groups, which supports (though does not prove) the assumption of a reasonably good sample from each group.

Also, there are a myriad of inherent limitations when performing functional imaging of the spinal cord (i.e. CSF pulsation and other physiological noise). The presence of these physiological contaminants could have adversely affected the diffusion signal thereby leading to artificially altered results. However, motion correction and outlier rejection techniques were applied to help mitigate these effects as detailed in Section 2.3. The preliminary nature of this study made some of these limitations difficult to avoid, however, the results shown are encouraging and these limiting factors are important questions to address for future work.

From an acquisition and image processing perspective, the manual ROI definition and slice thickness were also potential limitations. Previous work has demonstrated moderate to strong agreement for ROI placements in the pediatric spinal cord (Barakat et al., 2015). All ROIs were drawn for the whole cord in the axial plane containing both gray

and white matter as outlined in Section 2.4. The 6 mm slice thickness was required to maximize signal given the sub-millimeter in-plane resolution. Higher field strength, stronger gradients, more RF receive channels, and/or multiband imaging would have enabled smaller cuts while providing comparable, if not more, SNR.

5. Conclusion

In conclusion, statistically significant differences were seen for MK, Krad, Drad, and FA. The FA results yielded confidence that DKI data sets can reproduce trends seen in DTI for the pediatric spinal cord while MK differences suggest a lesser degree of micromolecular structure in patients with spinal cord injury. The radial results also indicate that in plane diffusion has been more adversely affected by trauma than its axial counterpart which could represent the transectional nature of an injury (perpendicular to the long axis of the spinal cord). Of particular interest is the complementary nature of the significant results. The radial kurtosis tends to decrease in patients with SCI while the radial diffusion increases. The combination of both these results could potentially give rise to a more comprehensive biomarker than either investigated individually. This is one particular area that needs to be studied in more depth by looking at the interaction of these radial components for patients in relation to healthy subjects. The results shown do demonstrate that DKI can not only replace conventional DTI in terms of functionality but offer additional information of clinical relevance that can more completely characterize the nature of water diffusion in pathologic and/or injured tissue.

References

Barakat, N., Hunter, L.N., Finsterbusch, J., Gaughan, J.P., Samdani, A.F., Mulcahey, M.J., Betz, R.R., Faro, S.H., Mohamed, F.B., 2011. Diffusion tensor imaging of the pediatric spinal cord using an inner-FoV EPI pulse sequence in normals and patients with SCI. Proceedings of the Annual Meeting of the International Society of Magnetic Resonance in Medicine (ISMRM), p. 400.

Barakat, N., Shah, P., Faro, S.H., Gaughan, J.P., Middleton, D., Mulcahey, M.J., Mohamed, F.B., 2015. Inter- and intra-rater reliability of diffusion tensor imaging parameters in the normal pediatric spinal cord. World J. Radiol. 7 (9), 279–285 (Available: http://www.ncbi.nlm.nih.gov/pmc/articles/PMC4585951/).

Bester, M., Sigmund, E.E., Tabesh, A., Jaggi, H., Inglese, M., Mitnick, R.J., 2010. Diffusional kurtosis imaging of the cervical spinal cord in multiple sclerosis patients. Proceedings of the 2010 Annual Meeting of ISMRM. Stockholm, Sweden.

Chang, L., Jones, D.K., Pierpaoli, C., 2005. RESTORE: robust estimation of tensors by outlier rejection. Magn. Reson. Med. 53 (5), 1088–1095.

Cohen, Y., Assaf, Y., 2002. High b-value q-space analyzed diffusion-weighted MRS and MRI in neuronal tissues — a technical review. NMR Biomed. 15 (7–8), 516–542.

Finsterbusch, J., 2009. High-resolution diffusion tensor imaging with inner field-of-view EPI. J. Magn. Reson. Imaging 29, 987–993.

Hori, M., Fukunaga, I., Masutani, Y., Taoka, T., Kamagata, K., Suzuki, Y., Aoki, S., 2012. Visualizing non-Gaussian diffusion: Clinical application of q-space imaging and diffusional kurtosis imaging of the brain and spine. Magn. Reson. Med. Sci. 11 (4), 221–233.

Hori, M., Tsutsumi, S., Yasumoto, Y., Ito, M., Suzuki, M., Tanaka, F.S., Kyogoku, S., Nakamura, M., Tabuchi, T., Fukunaga, I., Suzuki, Y., Kamagata, K., Masutani, Y., Aoki, S., 2014. Cervical spondylosis: Evaluation of microstructural changes in spinal cord white matter and gray matter by diffusional kurtosis imaging. Magn. Reson. Imaging 32 (5), 428–432.

Jansen, J.F., Stambuk, H.E., Koutcher, J.A., Shukla-Dave, A., 2010. Non-Gaussian analysis of diffusion-weighted MR imaging in head and neck squamous cell carcinoma: A feasibility study. AJNR Am. J. Neuroradiol. 31 (4), 741–748.

Jensen, J.H., Helpern, J.A., 2003. Quantifying non-Gaussian water diffusion by means of pulsed-field-gradient MRI. < br />. Proceedings of the 11th Annual Meeting of ISMRM; Toronto, Canada vol. 2154.

Jensen, J.H., Helpern, J.A., 2010. MRI quantification of non-Gaussian water diffusion by kurtosis analysis. NMR Biomed. 23 (7), 698–710 (Available: http://www.ncbi.nlm.nih.gov/pmc/articles/PMC2997680/).

Jensen, J.H., Helpern, J.A., Ramani, A., Lu, H., Kaczynski, K., 2005. Diffusional kurtosis imaging: the quantification of non-Gaussian water diffusion by means of magnetic resonance imaging. Magn. Reson. Med. 53 (6), 1432–1440.

Latt, J., Nilsson, M., Wirestam, R., Johansson, E., Larsson, E.M., Stahlberg, F., Brockstedt, S., 2008. In vivo visualization of displacement-distribution-derived parameters in q-space imaging. Magn. Reson. Imaging 26 (1), 77–87.

Lazar, M., Jensen, J.H., Xuan, L., Helpern, J.A., 2008. Estimation of the orientation distribution function from diffusional kurtosis imaging. Magn. Reson. Med. 60 (4), 774–781.

Li, X., Gao, J., Hou, X., Chan, K.C., Ding, A., Sun, Q., Wan, M., Wu, E.X., Yang, J., 2012. Diffusion kurtosis imaging with tract-based spatial statistics reveals white matter alterations in preschool children. Conf. Proc. IEEE Eng. Med. Biol. Soc. 2012, pp. 2298–2301.

Lu, H., Jensen, J.H., Ramani, A., Helpern, J.A., 2006. Three-dimensional characterization of non-Gaussian water diffusion in humans using diffusion kurtosis imaging. NMR Biomed. 19 (2), 236–247.

Middleton, D.M., Mohamed, F.B., Barakat, N., Hunter, L.N., Shellikeri, S., Finsterbusch, J., Faro, S.H., Shah, P., Samdani, A.F., Mulcahey, M.J., 2014. An investigation of motion correction algorithms for pediatric spinal cord DTI in healthy subjects and patients with spinal cord injury. Magn. Reson. Imaging 32 (5), 433–439.

Paydar, A., Fieremans, E., Nwankwo, J.I., Lazar, M., Sheth, H.D., Adisetiyo, V., Helpern, J.A., Jensen, J.H., Milla, S.S., 2014. Diffusional kurtosis imaging of the developing brain. AJNR Am. J. Neuroradiol. 35 (4), 808–814.

Pentang, G., Lanzman, R.S., Heusch, P., Muller-Lutz, A., Blondin, D., Antoch, G., Wittsack, H.J., 2014. Diffusion kurtosis imaging of the human kidney: a feasibility study. Magn. Reson. Imaging 32 (5), 413–420.

Raz, E., Bester, M., Sigmund, E.E., Tabesh, A., Babb, J.S., Jaggi, H., Helpern, J., Mitnick, R.J., Inglese, M., 2013. A better characterization of spinal cord damage in multiple sclerosis: a diffusional kurtosis imaging study. AJNR Am. J. Neuroradiol. 34 (9), 1846–1852.

Rieseberg, S., Frahm, J., Finsterbusch, J., 2002. Two-dimensional spatially-selective RF excitation pulses in echo-planar imaging. Magn. Reson. Med. 47 (6), 1186–1193.

Rosenkrantz, A.B., Prabhu, V., Sigmund, E.E., Babb, J.S., Deng, F., Taneja, S.S., 2013. Utility of diffusional kurtosis imaging as a marker of adverse pathologic outcomes among prostate cancer active surveillance candidates undergoing radical prostatectomy. Am. J. Roentgenol. 201 (4), 840–846. http://dx.doi.org/10.2214/AJR.12.10397.

Tabesh, A., Jensen, J.H., Ardekani, B.A., Helpern, J.A., 2011. Estimation of tensors and tensor-derived measures in diffusional kurtosis imaging. Magn. Reson. Med. 65 (3), 823–836.

Wilm, B.J., Svensson, J., Henning, A., Pruessmann, K.P., Boesiger, P., Kollias, S.S., 2007. Reduced field-of-view MRI using outer volume suppression for spinal cord diffusion imaging. Magn. Reson. Med. 57 (3), 625–630.

Wilm, B.J., Gamper, U., Henning, A., Pruessmann, K.P., Kollias, S.S., Boesiger, P., 2009. Diffusion-weighted imaging of the entire spinal cord. NMR Biomed. 22 (2), 174–181.

Yoshida, M., Hori, M., Yokoyama, K., Fukunaga, I., Suzuki, M., Kamagata, K., Shimoji, K., Nakanishi, A., Hattori, N., Masutani, Y., Aoki, S., 2013. Diffusional kurtosis imaging of normal-appearing white matter in multiple sclerosis: preliminary clinical experience. Jpn. J. Radiol. 31 (1), 50–55.

Zhang, Y., Yan, X., Gao, Y., Xu, D., Wu, J., Li, Y., 2013. A preliminary study of epilepsy in children using diffusional kurtosis imaging. Clin. Neuroradiol. 23 (4), 293–300.